Elastic scattering of 318 MeV ^{6}Li from ^{12}C and ^{28}Si: Unique phenomenological and folding-model potentials

A. Nadasen, T. Stevens, J. Farhat, and J. Brusoe
University of Michigan, Dearborn, Michigan 48128

P. Schwandt
Indiana University, Bloomington, Indiana 47405

J. S. Winfield, G. Yoo, and N. Anantaraman
National Superconducting Cyclotron Laboratory, Michigan State University, East Lansing, Michigan 48824

F. D. Becchetti, J. Brown, B. Hotz, J. W. Jänecke, and D. Roberts
University of Michigan, Ann Arbor, Michigan 48109

R. E. Warner
Oberlin College, Oberlin, Ohio 44074
(Received 27 July 1992)

The cross sections for elastic scattering of 318 MeV ^{6}Li from ^{12}C and ^{28}Si were measured. The data extend well beyond the rainbow angle into the region where the far-side scattering dominates, and thus define unique ^{6}Li phenomenological potentials. These complement earlier unique ^{6}Li potentials derived at an energy of 210 MeV. Double-folded real potentials also were generated using effective nucleon-nucleon interactions. The M3Y and Franey-Love 50 MeV nucleon-nucleon interactions gave similar potentials. A Woods-Saxon form was used for the imaginary potential. The experimental cross-section data were reasonably well reproduced without renormalization of the folded potentials.

PACS number(s): 25.70.Bc, 24.10.Ht, 24.50.+g

I. INTRODUCTION

The general applicability of semimicroscopic folding-potential models to the scattering of composite projectiles has been a subject of study for several decades. Comparison of the potentials for light ions such as ^{4}He and ^{6}Li with those of light heavy ions (e.g., ^{12}C and ^{16}O) should provide a more systematic insight into the validity, limitations, and relative merit of the various folding approaches as a function of projectile mass. Specifically, these investigations are meant to provide information on density-dependent effects in nuclear interactions of increasingly complex scattering systems, leading to appropriate refinements of the simple folding models [1–3].

The calculation of complex-projectile optical potentials using the single-nucleon optical potential and a detailed model for the projectile generally becomes more difficult as the number of nucleons in the projectile increases. Therefore, for ^{6}Li, advantage has been taken of its well-understood cluster structure, in particular the dominant, weakly bound $\alpha+d$ configuration. The ^{6}Li optical potential has been calculated to lowest order by convolution of the α-nucleus and d-nucleus potentials with the $\alpha+d$ cluster-model wave function [4–6]. On the other hand, double-folding calculations generated from the fundamental nucleon-nucleon interactions have also been carried out [7,8], but they do not generally incorporate nuclear structure effects. All previous calculations have been found to overestimate the strength of the potentials [9]. These calculations neglect distortion effects, the Pauli exclusion principle, and breakup of the projectile. Attempts [10] to account for projectile breakup by introducing a repulsive potential seem to correct some of the deficiencies, but there still remain questions about the validity of such a formalism.

It is clear that the folding-model calculations for ^{6}Li elastic scattering require additional refinements. Evaluation of these calculations and determination of their deficiencies have previously been obscured by the existence of discrete ambiguities in phenomenological optical-model (OM) potentials [6,11]. These ambiguities can be eliminated by making elastic-scattering measurements at higher energies over sufficiently wide angular ranges; cross sections extending beyond the so-called "rainbow" angle into the region dominated by far-side scattering are needed to determine unique ^{6}Li-nucleus OM potentials. At low energies, where the rainbow occurs at rather large angles, the rapid decrease in cross section with angle precluded such measurements [6,11].

Recent ^{6}Li elastic-scattering measurements over wide angular ranges have provided unique phenomenological OM potentials for ^{12}C, ^{28}Si, ^{40}Ca, ^{58}Ni, and ^{90}Zr at 210 MeV [12,13]. These data form a basis for evaluation of microscopic calculations at these energies. However, for a global understanding of the ^{6}Li-nucleus interaction, additional measurements are needed; we have to unambigu-

ously define the energy and target-mass dependences of these unique OM potentials.

Therefore, we have measured, and report in this paper, differential cross sections for the elastic scattering of 318-MeV ^{6}Li from ^{12}C and ^{28}Si. The goal of these measurements was to determine unique ^{6}Li-nucleus OM potentials and, with the aid of earlier measurements, to derive an energy dependence of the unique potentials. These results will broaden our understanding of the ^{6}Li-nucleus interaction by providing systematics of the parametrization of the phenomenological OM potentials. The existence of unique potentials also facilitates unambiguous evaluations of microscopic folding-model calculations.

Section II describes the experimental procedure of the present experiment. The results of the measurements are presented in Sec. III. Section IV discusses the optical-model analyses of the data. Folding-model calculations for these and lower-energy data are given in Sec. V. Section VI contains the summary and conclusions.

II. EXPERIMENT

The elastic-scattering differential cross sections were measured using a 53 MeV/nucleon ^{6}Li beam from the K500 cyclotron of the National Superconducting Cyclotron Laboratory at Michigan State University. The uncertainty in the beam energy was estimated from cyclotron parameters to be 1%, and its energy resolution was of the order of 0.1%. The beam was focused on targets at the center of a 40-cm-diameter scattering chamber attached to the S-320 magnetic spectrometer. The beam spot on target was about 2 mm wide by 4 mm high. The beam line elements were carefully adjusted to minimize steering of the beam by the focusing quadrupoles. Further adjustments were carried out to eliminate beam halo. This was verified by the lack of detector counts when a blank target frame, having an opening equal to the smallest target used, was placed in the target position.

Targets used were 0.482 and 31.0 mg/cm^2 natural C (99% ^{12}C) and 5.8 and 32 mg/cm^2 natural Si (92% ^{28}Si). The scattered particles were observed with the S-320 spectrometer, which has a quadrupole-quadrupole-dipole-multipole configuration. The solid angle subtended by the entrance slits to the spectrometer ranged from 53 to 660 μsr, corresponding to horizontal angular acceptances of 0.2–1.48°. The narrowest slits were used in the region of diffractive oscillations where cross sections varied rapidly with angle. The broad slits were effective for obtaining acceptable statistics at the large angles, where the cross sections were small but appeared to exhibit a smooth exponential falloff.

The spectrometer focal-plane detection system consisted of two position-sensitive (by charge division) single-wire proportional counters, two ΔE ion chambers, and a stopping plastic scintillator. The scintillator provided the event trigger. The overall energy resolution was 0.2%, which was sufficient to resolve scattering to the first excited states from the ground states for the targets used. Particle identification was achieved by creating two-dimensional spectra of ΔE (ion chamber) versus E (plastic scintillator). These provided clean separation between the ^{6}Li and other particles of the same rigidity (mostly ^{4}He and ^{7}Li) that arrived in the focal plane. A window enclosing the ^{6}Li particles in the ΔE-E spectrum was used to gate the proportional-counter momentum spectrum, thus providing an energy spectrum of ^{6}Li.

The magnetic elements of the spectrometer were regularly adjusted to center the elastically scattered ^{6}Li on the focal plane, using values calculated from the S-320 kinematics for 53 MeV/nucleon ^{6}Li elastic scattering. This optimized the energy resolution and precluded effects of possible efficiency variation across the focal plane. The angular position of the spectrometer was read to a precision of better than 0.02° from a vernier scale on the spectrometer moving across a main scale attached to the circular track. The thin targets were used for the forward-angle measurements where the yield for elastic scatterings was large, and the low cross sections at large angles were measured with the thick targets. The beam current ranged from a fraction of a nanoampere to as high as 8 nA. At the forward angles, the beam current was controlled in order to keep the data-acquisition dead time below 10%. The dead time was monitored by feeding pulses at a random rate to the focal-plane detectors and processing them in the same manner as those from the real events in the detectors. The ratio of the number of pulses processed to those fed into the system was taken as the live time for each run and was used to correct the real data.

The beam currents were measured with two different Faraday cups. For angles $\geq 4°$, a counter-bored retractable Faraday cup, which was attached to the nonrotating part of the chamber and subtended an angle of 3°, was used. Because of the small solid angle available for secondary electron emission, the charge collected by this Faraday cup was accepted as the true value. For smaller angles, the charge was collected by a horizontal plate located 1.5 m from the target. This plate moved with the spectrometer. It allowed measurements down to 2°, but electron emission resulted in excess charge being indicated by this beam stop, as determined by overlap measurements between the two beam stops. This result was also confirmed by monitor counts. The overlap points were used to correct the charge collected by the horizontal plate.

Four photodiode monitors, 0.16 cm^2 in area, were located symmetrically around the beam, 15.6 cm downstream from the target. Each subtended a solid angle of 0.66 msr and made an angle of 11.5° with the beam. These were used to monitor changes in beam position and direction and the relative Faraday-cup charge collection efficiency. The monitor counts always scaled with the Faraday-cup readings and they showed no indication of beam direction or position changes. The monitors were also used for angle-offset determination in the comparison of yields on either side of the beam, because the Faraday cups could not be used for negative-angle measurements.

After each beam-line tuneup, the angle offset (usually $<0.1°$) of the beam was measured and the angles were corrected accordingly. Overlap data points were taken

whenever experimental conditions were changed, such as targets, slits, and current integrator scales. The overlap data for slits and integrator scales agreed within statistics. They were different for target changes. It was assumed that the value of the thick targets was correct, and the thin target cross sections were renormalized with the aid of the overlap data. The angle steps were carefully chosen so that the shape of the angular distribution could be well defined, particularly in the diffraction region. The criterion for each datum point was to obtain a statistical accuracy of 2% or a maximum data-acquisition time of 30 min.

During data acquisition, a sample of the data was analyzed online in order to monitor dead time, pileup, energy resolution, and changes in experimental conditions. The laboratory online cross sections were continually plotted as the experiment progressed to ensure that the shape of the angular distribution was well defined. All data were written event by event on magnetic tapes for later offline analysis. When the tapes were replayed, the elastic and inelastic peak areas were extracted from the position spectrum, gated by particle identification. They were also extracted by drawing two-dimensional windows on the PID-gated angle versus position spectrum. There was complete agreement between the two methods adopted. For unambiguous identification of the peaks, the separation between the ground-state and excited-state peaks were monitored. The position of the elastic peak was also compared to that expected from kinematics for the respective dipole magnet setting. The sum in the elastic peak was used to calculate the cross section for each angle.

III. RESULTS

The elastic-scattering angular distribution for the ^{12}C target is shown in Fig. 1. The measurements extend from 4 to 46° in the center of mass (c.m.) and cover eight orders of magnitude. Diffractive oscillations are observed only at the most forward angles ($\theta_{c.m.} < 20°$). The data beyond 20° are characterized by smooth exponential falloff, which shows the dominance of far-side scattering. These large-angle measurements are critical for the determination of unique phenomenological OM potentials [12,13]. The ^{28}Si data (shown in Fig. 2) extend from 4 to 39° c.m. and cover almost eight orders of magnitude. Because of the larger radius of the ^{28}Si, the oscillations are more compressed and have an oscillatory period of ~4°. One thus observes more oscillations in the angular range up to ~20°. Far-side scattering data covering about three orders of magnitude are sufficient to define unique potentials. Cross sections down to a fraction of μb were measured for both targets.

In determining relative errors, five different contributions were considered. (i) For most of the measurements, the statistical uncertainty was generally 1–3%. Only cross sections in the μb region had statistical uncertainties ~10%. (ii) Errors due to charge-integration efficiency were estimated to be 1–2%, depending on the current integrator scale used. (iii) The error introduced by the variation of beam position on the target (due to the finite size of the beam and nonuniformity in the target thickness) ranged from ~3% for the thin targets to ~0.5% for the thick targets. (iv) Dead times were kept below 10% by controlling the data-acquisition rates. Thus uncertainty in the dead-time correction contributed less than a 1% error to the cross section. (v) Uncertain-

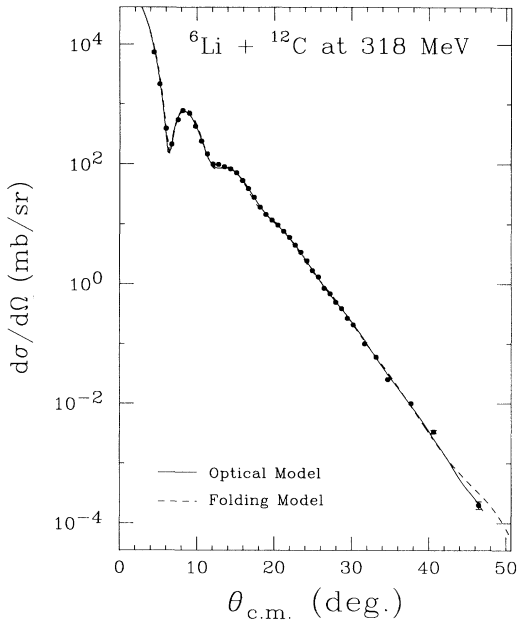

FIG. 1. Angular distribution of the differential cross sections for the elastic scattering of 318-MeV ^{6}Li from ^{12}C. The solid line represents the optical-model fit that provides the unique potential parameters listed in Table I. The dashed line represents the folding-model calculations. (See text.)

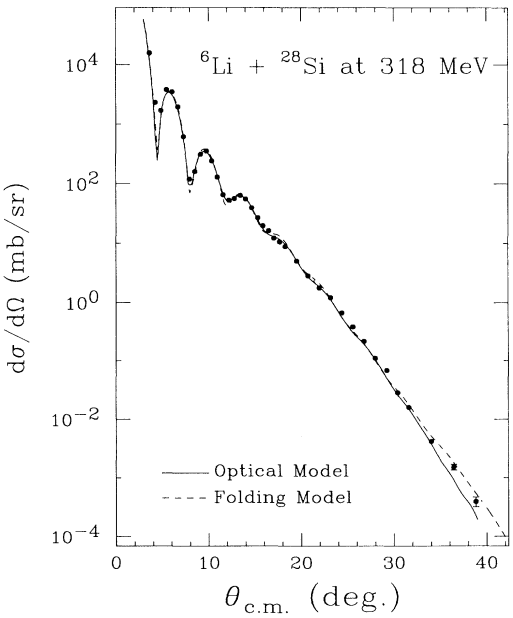

FIG. 2. Same as Fig. 1, but for the ^{28}Si target.

ties in the effective scattering angle, due to both uncertainties in the angle readout and variations in beam direction during the measurements, was estimated to be $\sim 0.04°$. This corresponds to cross-section errors from nearly zero to as high at 8%, depending on the slope of the angular distribution. The relative errors from all five sources were added in quadrature to obtain the total relative uncertainty for each datum point. However, repetition of measurements indicated that reproducibility of cross sections can only be achieved at the 3% level. Therefore, the minimum error of all data was set at 3%. These errors are displayed in Figs. 1 and 2 when they are larger than the data points.

Target-thickness uncertainty was the major contributor to the overall absolute (normalization) error of the data. The combined uncertainty from other sources such as detector efficiency, charge integration, spectrometer solid angle, and target angle was estimated at about 1%. The total normalization error was assumed to be $\pm 5\%$.

IV. OPTICAL-MODEL ANALYSES

The analyses of the data were carried out with the conventional nonrelativistic Schrödinger optical-model (OM) formalism, where it is assumed that the incident ^{6}Li waves are diffracted by a local central potential $U(r)$. Relativistic effects at this energy are expected to have a negligible effect on the calculations. A spin-orbit potential was not included, since it is well known that the differential cross-section data in this energy region are not sensitive to the spin-orbit interaction [8]. Further, the interplay between the spin-orbit potential and the nuclear central potential can obscure systematic information on the latter.

The calculations were carried out with the OM search program ECIS79 [14]. The analyses employed real and volume-imaginary central potentials together with a Coulomb potential. Inclusion of a surface-imaginary potential produced no significant improvement to the fits. The potential adopted was

$$U(r)=U_C(r,r_C)-Vf(r,r_0,a_0)-iW_v f(r,r_w,a_w)\ , \qquad (1)$$

where $f(r,r_x,a_x)$ is the Woods-Saxon form factor $\{1+\exp[(r-r_x A_t^{1/3})/a_x]\}^{-1}$ and $U_C(r,r_C)$ is the Coulomb potential due to a uniform sphere with charge equal to that of the target nucleus and radius $r_C A_t^{1/3}$.

The search program can be used to carry out searches on any combination of the six parameters in order to minimize χ^2, defined by

$$\chi^2=\sum_{i=1}^{N}\left[\frac{\sigma(\theta_i)^{\rm cal}-\sigma(\theta_i)^{\rm exp}}{\Delta\sigma(\theta_i)}\right]^2 , \qquad (2)$$

where N is the number of differential cross-section data points. $\sigma(\theta_i)^{\rm cal}$ is the ith calculated cross section. $\sigma(\theta_i)^{\rm exp}$ and $\Delta\sigma(\theta_i)$ are the corresponding experimental cross section and its relative uncertainty, respectively.

Starting parameters were obtained from the results of the 210-MeV analyses for these targets [12,13]. The strength of the real potential was scaled down to account for the expected energy dependence. Initial searches were made in sequence on each of the six parameters. This was followed by all possible combinations of two parameters. Then three-parameter combinations were searched on. As the fit improved, the number of parameters in the search was increased until final searches were carried out on all parameters. At this stage, a surface-imaginary term was introduced. While it modified the existing parameters somewhat, it produced no noticeable improvement either in terms of the χ^2 criterion or visual fit to the data. It was therefore discarded. Once reasonably acceptable fits were obtained, the absolute normalization of the data was allowed to vary. These calculations indicated no preference for a change in normalization.

In order to determine whether the potentials were indeed unique, grid searches were then made. Starting with the best-fit six parameters, the strength V of the real potential was gridded in 5-MeV steps, while searching on the other five parameters. The value of χ^2 increased monotonically as the value of V was increased from the best-fit value. This was also true when V was decreased to values less than the best-fit value. No other minimum in χ^2 was found for values of V from 20 to 500 MeV. This procedure provided sufficient evidence that the data selected *single unique potentials*. The final parameters thus obtained are listed in Table I. The fits to the data are shown as solid lines in Figs. 1 and 2.

Table I shows that the volume integral of the real potential for ^{12}C is larger than that for ^{28}Si. This is in agreement with the results at 210 MeV where it was found that the volume integrals had an $A^{-1/3}$ dependence on the target mass. The overall fits to the data (Figs. 1 and 2) are extremely good. The calculations reproduce the cross sections rather well in the diffraction region. The agreement between the calculations and the data in the smooth exponential falloff region extends down to cross sections of less than a μb.

Using these potentials and those at 210 MeV, an energy dependence of the real volume integrals was derived. In this procedure potentials at lower energies identified as belonging to the unique families were also included (see Refs. [12,13]). These values are shown in Figs. 3 and 4. An uncertainty of 5% was assigned to all volumes integrals, and least-squares fits to the data were made.

TABLE I. Unique OM potential parameters for elastic scattering of 318-MeV ^{6}Li ions from ^{12}C and ^{28}Si. The convention $R_x=r_x A_t^{1/3}$ is used.

Target	V (MeV)	r_0 (fm)	a_0 (fm)	W_v (MeV)	r_w (fm)	a_w (fm)	$J_R/6A_t$ (MeV fm^3)	$J_w/6A_t$ (MeV fm^3)	σ_R (mb)	χ^2/N
^{12}C	126.9	1.136	0.897	29.3	1.695	0.878	285	150	1082	3.0
^{28}Si	117.6	1.292	0.874	40.6	1.595	0.772	264	141	1457	3.5

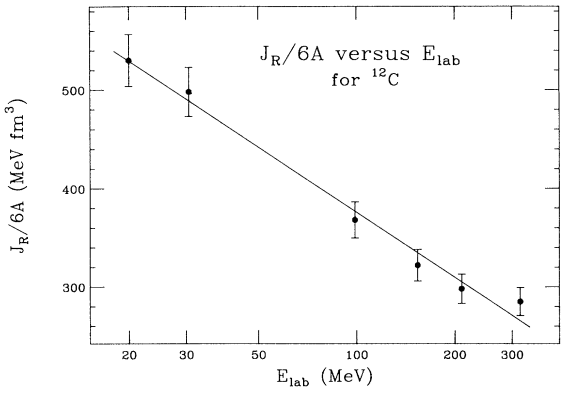

FIG. 3. Energy dependence of the real potential volume integral per nucleon pair for the elastic scattering of ^{6}Li from ^{12}C. The straight line represents the derived energy dependence.

These are shown by the straight lines in Figs. 3 and 4. Thus, a logarithmic dependence on the bombarding energy of the form

$$J_R/6A = J_R^0/6A - \beta \ln E_{\rm lab} \quad (3)$$

was obtained for each target, where $E_{\rm lab}$ is in units of MeV. For ^{28}Si, $J_R^0/6A = 840 \pm 30$ MeV fm^3 and $\beta = 103 \pm 5$ MeV fm^3 were obtained. The corresponding values for ^{12}C were $J_R^0/6A = 815 \pm 30$ MeV fm^3 and $\beta = 95 \pm 5$ MeV fm^3.

V. FOLDING-MODEL CALCULATIONS

The double-folding potentials were calculated for the real part of the ^{6}Li-nucleus interaction following the method given by Satchler and Love [7]. In their description, the folded potential can be written as

$$U_F(R) = \int d\mathbf{r}_1 \int d\mathbf{r}_2 \rho_1(\mathbf{r}_1)\rho_2(\mathbf{r}_2)v(r_{12}) , \quad (4)$$

where $v(r_{12})$ is the two-body nucleon-nucleon interaction, and ρ_1 and ρ_2 are the distributions of the centers of mass of the nucleons in the ground state of the two nuclei for which the folding potential is calculated. The folding-model potentials were calculated using the program FOLD [15]. These potentials were then used in the calculations of 318-MeV ^{6}Li elastic scattering from ^{12}C and ^{28}Si. A volume Woods-Saxon form was used for the imaginary potentials. Its initial parameters were obtained from the phenomenological results and were adjusted to fit the data.

Two different nucleon-nucleon interactions were used. One was the effective interaction of Bertsch *et al.* [16], known as M3Y, which is expressed as a sum of three Yukawa terms. They represent the attractive, long-range one-pion exchange, medium-range multiple-pion exchange, and a short-range repulsive interaction. The other was the 50-MeV Franey-Love [17] interaction. It was found that the calculations were not sensitive to the type of nucleon-nucleon interaction employed, and both forces provided very similar folded potentials. The potentials were more sensitive to the wave functions assumed for the transition density. Both harmonic-oscillator (H.O.) and Woods-Saxon (WS) single-particle wave functions were used to construct the density distributions $\rho_1(\mathbf{r}_1)$ and $\rho_2(\mathbf{r}_2)$ of ^{6}Li and the target in Eq. (4). For the H.O. wave functions, the oscillator constant α in $\exp(-\alpha r^2)$ was initially adjusted to give density distributions with a root-mean-square radius equal to that found empirically by electron scattering [18]. Potentials generated by these density distributions did not give good fits to the data. Then α was allowed to vary as a free parameter in order to optimize the fits to the data. The best-fit value of α gave a rms radius of ^{6}Li, which was $\sim 20\%$ smaller than the electron-scattering result. On the other hand, when WS single-particle wave functions were used, the calculated potentials were very similar to empirically determined unique potentials, and a more realistic ^{6}Li rms radius was obtained. The geometry parameters for the Woods-Saxon well were $r_0 = 1.25$ fm and $a_0 = 0.65$ fm. The strength V was adjusted to give the single-particle separation energies. In Fig. 5 we compare the potentials

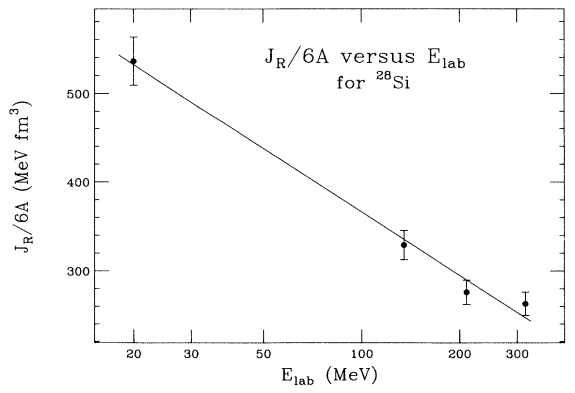

FIG. 4. Same as Fig. 3, but for the ^{28}Si target.

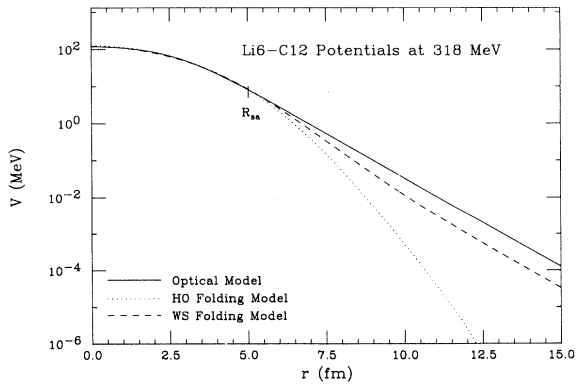

FIG. 5. ^{6}Li+^{12}C double-folded real potential, using the Woods-Saxon (dashed line) and harmonic-oscillator (dotted line) wave functions for the transition densities. The solid line represents the unique phenomenological OM potential. The R_{sa} is the strong absorption radius.

derived using the harmonic-oscillator and Woods-Saxon wave functions with the unique phenomenological potential for ^{6}Li+^{12}C. Note that the potentials agree quite well for $r \leq R_{sa}$, the strong absorption radius. Beyond R_{sa} the potential generated with the adjusted H.O. wave functions falls off much more rapidly than either the potential generated from the WS wave functions or the purely phenomenological potential, a reflection of the unrealistic large-r behavior of the H.O. wave function. The final results of the folding-model calculations are given in Figs. 1 and 2 as dashed lines. (The solid lines represent the calculations of the unique phenomenological real potentials.) It is apparent that the folding-model calculations reproduce the differential cross sections almost as well as the unique potentials. It is significant that *no renormalization* of the folded potential was necessary to obtain the good agreement. In fact, attempts were made to verify if the potential normalized by a factor of less than unity would reproduce the data. The potential was normalized by $N=0.6$ and a search was carried out by varying the parameters of the imaginary potential. The fits were unsatisfactory, with χ^2 being about a factor of 10 higher than that of the $N=1$ potential. The calculations deviated significantly from the data for the larger angles. As a check of our procedure and to ensure that no hidden normalization factor was present in our code, we attempted to reproduce the folding potential for ^{6}Li+^{26}Mg at 36 MeV given by Woods *et al.* [9]. We generated a potential for their system, renormalized it by 0.6, as they did, and found that the fit to the data was comparable to theirs.

Folding-model calculations were also carried out for data at lower energies at which unique OM potentials were identified [12,13]. The same folding-model prescriptions were used at all energies. Figures 6 and 7 show that the calculations for ^{12}C and ^{28}Si at 210 MeV [12,13] provide reasonably good fits to the experimental data, although the phenomenological fits are somewhat superior. The calculations for ^{40}Ca at 210 MeV [13] (Fig. 8) deviate from the data at large angles. This seems to indicate that the folding-model calculations are valid for light targets, but have difficulty reproducing cross sections for heavier targets. Higher-order corrections to the folding-model

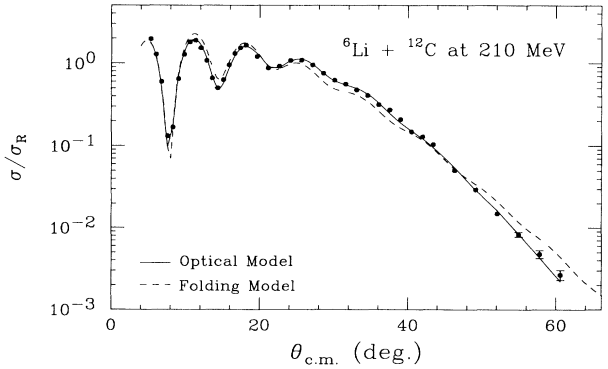

FIG. 6. Comparison of folding-model calculations (dashed line) with those of the unique OM potentials (solid line) for ^{6}Li+^{12}C at 210 MeV.

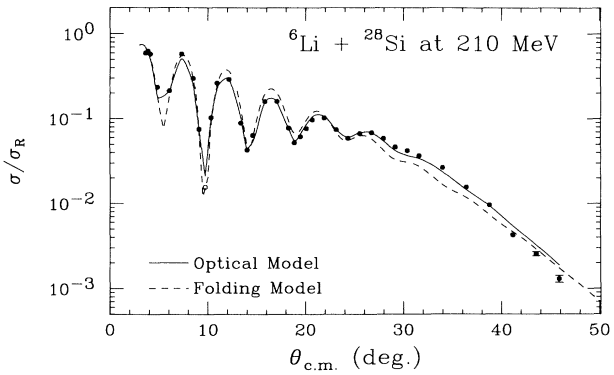

FIG. 7. Same as Fig. 6, but for ^{6}Li+^{28}Si at 210 MeV.

calculations may be necessary for the heavier targets, probably due to the mixed configuration of the ground-state wave functions. In this regard there have been suggestions that 2p-2h (two-particle–two-hole) and 4p-4h states had non-negligible contributions to the ground-state wave function of ^{40}Ca [19].

Figure 9 shows the calculations for the ^{12}C target at 99 MeV. In the phenomenological OM analysis of these data, several sets of potentials belonging to different discrete families were obtained [6]. However, using the energy dependence of the unique potentials obtained at 210 and 318 MeV, the potentials parameters with the real volume integral per nucleon pair 368 MeV fm^3 were chosen as belonging to the unique family. This potential was then used for evaluating the folding-model calculation. The folded potential generated was, in fact, very similar to the real part of this phenomenological potential. Although the fit to the data is somewhat inferior, it compares well with the results of the renormalized folded potentials initially carried out (see Fig. 2 of Ref. [8]).

The main theme of our folding-model calculations is that the existence of a unique phenomenological OM potential facilitates unambiguous evaluation of folding-model calculations. Since only a single potential is generated in a folding calculation, the appropriate OM potential to compare it with is the unique potential. One

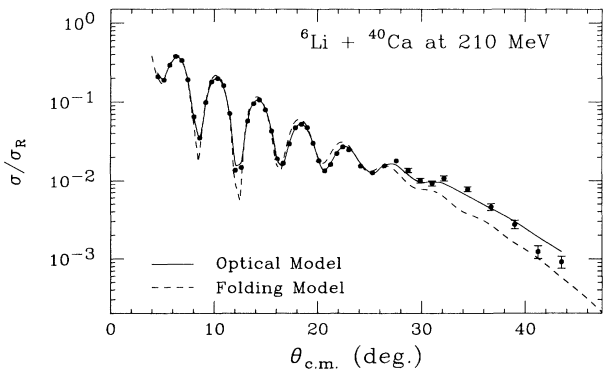

FIG. 8. Same as Fig. 6, but for ^{6}Li+^{40}Ca at 210 MeV.

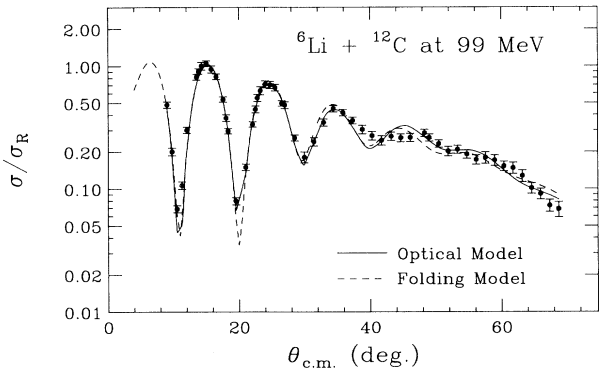

FIG. 9. Same as Fig. 6, but for ^{6}Li+^{12}C at 99 MeV.

may renormalize the folded potential to mimic one of the other ambiguous OM potentials, but this becomes unnecessary if the unique OM potential is known.

VI. SUMMARY AND CONCLUSIONS

Differential cross sections for the elastic scattering of 318-MeV ^{6}Li ions from ^{12}C and ^{28}Si have been measured. The data extend to 46° for ^{12}C and 39° for ^{28}Si in the center-of-mass system. The cross sections span over eight orders of magnitude, with the lowest cross sections being less than 1 μb. The angular range of measurements was sufficient to determine unique phenomenlogical ^{6}Li-nucleus OM potentials at 318 MeV.

Together with our results at 210 MeV and selected analyses of lower energy data [6,20–23], an energy dependence of the potentials for each target was obtained. The combined results indicate that the ^{6}Li-nucleus real volume integral has a logarithmic dependence on bombarding energy of the form $J_R/6A = J_R^0/6A - \beta \ln E_{lab}$, with $J_R^0/6A = 830 \pm 30$ MeV fm^3 and $\beta = 100 \pm 5$ MeV fm^3. This is in good agreement with our earlier results that used data extending up to 210 MeV [12,13], and is consistent with the energy dependences for proton [24,25] and α [26] elastic scattering. If the ^{6}Li energy dependence is extrapolated to higher energies, the potential would become zero at around 600 MeV/nucleon. This compares well with the analyses of proton and α elastic scattering, which predict a change in the sign of the real potential at about the same energy per nucleon, if a monotonic potential shape (e.g., Woods-Saxon) if assumed [27].

The imaginary volume integrals of 141 MeV fm^3 for ^{28}Si and 150 MeV fm^3 for ^{12}C are consistent with the results at 210 MeV and lower energies. For ^{6}Li elastic scattering the imaginary volume integrals have been found to range from ~100 to ~150 MeV fm^3 with no indication of any systematic dependence on the bombarding energy [12,13]. However, they do show an $A^{-1/3}$ dependence on the target mass, which is supported by the present results. Total reaction cross sections of 1082 mb (for ^{12}C) and 1457 mb (for ^{28}Si) were calculated from the derived optical-model potentials. They are close enough to the values of 1090 and 1641, respectively, deduced at 210 MeV [13], to conclude that the total ^{6}Li reaction cross section is essentially independent of energy in this energy region.

A more fundamental analysis of the data involved semimicroscopic folding-model calculations. The real part of the potentials for ^{6}Li elastic scattering was generated by means of a complete double-folding procedure, using fundamental nucleon-nucleon interactions. The calculations seem to be insensitive to the two types of nucleon-nucleon interactions employed. However, they clearly show a preference for Woods-Saxon wave functions in the calculation of the transition densities.

The calculations at all three energies (99, 210, and 318 MeV) provide potentials very similar to the unique phenomenological OM potentials. (See Fig. 10 for ^{6}Li+^{12}C potentials at 210 MeV.) They reproduce the experimental data almost as well as the phenomenological analyses without renormalization of the potentials. This is in contrast to previous lower-energy analyses [7–9], where it was found that a renormalization by 0.5–0.7 of the folded potential was necessary to fit the elastic-scattering data. The Woods-Saxon imaginary potentials used with the folded real potentials are also not very different from those obtained with the phenomenological analyses.

In retrospect, it appears that the existence of many families of discrete ambiguous potentials was responsible for the difficulties encountered in folding-model analyses of elastic-scattering data. Since many different phenomenological potentials could fit the elastic-scattering data, the renormalization resulted in mimicking one of the shallower ambiguous potentials. One has to realize that because of the extreme surface localization of the scattering process at the lower energies, agreement at the tail of the potential will be sufficient to reproduce the data. In our reanalysis of the 36-MeV ^{6}Li+^{26}Mg data [9], we were able to fit the data with the folded potential normalized by 0.6. This implies that the renormalization of the double-folded potential for ^{6}Li is energy dependent at energies well above the Coulomb barrier. In view of the existence of additional ambiguous families at lower energies, it will be interesting to explore whether other nor-

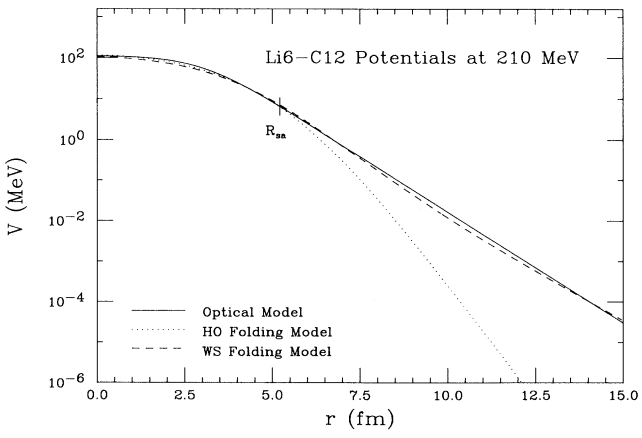

FIG. 10. Same as Fig. 5, but for ^{6}Li+^{12}C at 210 MeV.

malizations would reproduce the experiment data. In fact, Woods *et al.* [9] found that three different normalizations (possibly corresponding to three ambiguous families) provided equally good fits to their ^{6}Li and ^{16}O data.

Once the scattering data identify a unique phenomenological OM potential, folding-model calculations have an unambiguous potential for comparison. Therefore, it seems appropriate to conclude that the existence of unique phenomenologial OM potentials be a prerequisite for reliable evaluation of folding-model calculations of the nuclear interior.

ACKNOWLEDGMENTS

We wish to thank the cyclotron staff of the National Superconducting Cyclotron Laboratory (NSCL) for the high-quality ^{6}Li beams provided for this experiment. This work was supported in part by the National Science Foundation under Grant Nos. PHY 9111710 (UM, Dearborn), PHY 9015957 (IUCF), PHY 8913815 (NSCL), PHY 9122067 (Oberlin College), and PHY 8911831 (UM, Ann Arbor).

[1] D. F. Jackson and V. K. Kembhavi, Phys. Rev. **178**, 1626 (1969).
[2] A. Budzanowski *et al.*, Phys. Lett. **32B**, 431 (1970).
[3] J. P. Vary and C. B. Dover, Phys. Lett. **59B**, 121 (1975).
[4] J. W. Watson, Nucl. Phys. **A198**, 129 (1972).
[5] J. Jänecke, F. D. Becchetti, and D. Overway, Nucl. Phys. **A343**, 161 (1980).
[6] P. Schwandt *et al.*, Phys. Rev. C **24**, 1522 (1981).
[7] G. R. Satchler and W. G. Love, Phys. Rep. **55**, 183 (1979).
[8] D. P. Stanley, F. Petrovich, and P. Schwandt, Phys. Rev. C **22**, 1357 (1980).
[9] C. L. Woods, B. A. Brown, and N. A. Jelley, J. Phys. G. **8**, 1699 (1982).
[10] Y. Sakuragi, M. Yahiro, and M. Kamimura, Prog. Theor. Phys. **68**, 322 (1982); **70**, 1047 (1983); Y. Sakuragi, M. Kimimura, S. Micek, H. Rebel, and H. J. Gils, Z. Phys. **322**, 627 (1985); K. Katori *et al.*, Nucl. Phys. **A480**, 323 (1988).
[11] J. Cook, Nucl. Phys. **A388**, 153 (1982).
[12] A. Nadasen *et al.*, Phys. Rev. C **37**, 132 (1988).
[13] A. Nadasen *et al.*, Phys. Rev. C **39**, 536 (1989).
[14] J. Raynal, computer code ECIS79, Centre d'Etudes Nucléaires, Saclay, France, 1979.
[15] J. Cook and J. A. Carr, computer program FOLD, Florida State University, Tallahassee, FL, 1988.
[16] G. Bertsch, J. Borysowicz, H. McManus, and W. G. Love, Nucl. Phys. **A284**, 399 (1977).
[17] M. A. Franey and W. G. Love, Phys. Rev. C **31**, 488 (1985).
[18] C. W. De Jager, H. De Vries, and C. De Vries, At. Data Nucl. Data Tables **14**, 479 (1974).
[19] T. A. Carey, P. G. Roos, N. S. Chant, A. Nadasen, and H. L. Chen, Phys. Rev. C **23**, 576 (1981).
[20] J. W. Watson, Nucl. Phys. **A198**, 129 (1972).
[21] P. Schumacher, N. Ueta, H. H. Duhm, K.-I. Kubo, and W. J. Klages, Nucl. Phys. **A212**, 573 (1973).
[22] R. M. DeVries, D. A. Goldberg, J. W. Watson, M. S. Zisman, and J. G. Cramer, Phys. Rev. Lett. **39**, 450 (1977).
[23] J. Cook, H. J. Gils, H. Rebel, Z. Majka, and H. Klewe-Nebenius, Nucl. Phys. **A388**, 173 (1982).
[24] A. Nadasen *et al.*, Phys. Rev. C **23**, 1023 (1981).
[25] P. Schwandt, in *The Interaction Between Medium Energy Nucleons in Nuclei,* Proceedings of the Workshop on the Interactions Between Medium Energy Nucleons in Nuclei, edited by H. O. Meyer, AIP Conf. Proc. No. 97 (AIP, New York, 1982), p. 89.
[26] A. Nadasen, P. G. Roos, N. S. Chant, C. C. Chang, and T. A. Carey, Bull. Am. Phys. Soc. **26**, 580 (1981); A. Nadasen and P. G. Roos, *ibid.* **29**, 1040 (1984).
[27] In a more realistic picture, density dependence and/or relativity force the interior of the nucleon potential to become more repulsive at a much lower energy, while maintaining an attractive surface region up to about 600 MeV.